



than what is required to explain the deficit of 30-m-diameter craters on Eros. Moreover, at a global scale, the behavior of the depleted crater population of Eros is a  $D^{-2.5}$  function of crater size, whereas the size dependency of the Yarkovsky drift is only  $D^{-0.5}$ . Thus, the Yarkovsky effect cannot explain the deficit of small craters according to Bottke et al. [2000]. This is further confirmed by O'Brien and Greenberg [2007], who suggested that to reproduce a main belt size distribution suitably depleted in small impactors to match the small crater population of Eros, a much higher size-dependent removal rate than the Yarkovsky effect is required. Finally, if we assume that the inner Solar system (including the Main Asteroid Belt and Eros) was impacted by a standard projectile population function, the crater population of Eros must have been shaped by one or several erasure processes [Chapman et al., 2002].

[4] Erasure processes suggested to explain the lack of small craters on Eros include seismic shaking [Richardson et al., 2005], electrostatic dust levitation leading to the formation of ponded deposits [Asphaug, 2004] or ejecta blanketing [Robinson et al., 2002]. The observed crater population of Eros is well explained by an erasure model implying impact-induced seismic shaking along with a preliminary model of ejecta coverage [Richardson et al., 2005]. In that process, seismic vibrations are produced by impacts and trigger downslope movements on crater walls. Although no estimate of the contribution of the ejecta blanketing process (relative to the seismic shaking contribution) is available, the simulations of Richardson et al. [2005] suggest a main belt exposure age of 400 Ma for the surface of Eros.

[5] The amplitude of seismic waves is however very sensitive to the regolith structure, because of its very low seismic velocities, which trap the waves near the surface. Such sensitivity was for example found on the Moon: signals arriving at the Apollo 15 site were amplified by a factor of 1.5 relative to the Apollo 12 site, and for the Apollo 14 and 16 sites, the amplification factor was even higher: 3.5 [Nakamura et al., 1975; Horvath et al., 1980]. These differences are associated to the variation of the regolith layers. The first layer for example, associated to young regolith composed of porous, highly fractured and brecciated rocks, was between 2 and 12 m thick on the different Apollo landing sites. The other deeper layers vary in a relatively similar way [see Lognonné and Mosser, 1993] but are associated to larger regolith blocks. We therefore expect seismic shaking to be sensitive to the local structure of the regolith. Size-frequency curves of small bodies may therefore carry information about the small body subsurface, which might remain unique until seismic investigations are carried out by future missions (see, for instance, Lognonné [2005] and Lognonné and Johnson [2007] for recent reviews of planetary and small body seismology).

[6] Such a perspective however requires an accurate modeling of all effects possibly erasing craters, in order to extract with confidence the effects of the regolith on the structure. Such improved modeling is not only required for seismic shaking but also for all mechanisms erasing craters, including those that were expected to generate a smaller

effect, such as ejecta coverage, which was simulated in a simple and preliminary way by Richardson et al. [2005].

[7] Another hypothesis is the occurrence of ponded deposits [Asphaug, 2004] formed by electrostatic dust levitation since Eros became a Near Earth Asteroid (indeed, the distribution of these ponds suggests that a high solar flux is required for electrostatic processes to occur, and such a flux can be found on a Near Earth Asteroid orbit).

[8] It can also be proposed that the regolith deposition created by reimpacting ejecta resulting from impacts [Durda, 2004] contributes to crater erasure and particularly affects small craters by burial [Robinson et al., 2002]. This ejecta blanketing erasure process would result in smoothing of the crater rims [Robinson et al., 2002], a process that can also be induced by regolith maturation [Robinson et al., 2001]. Consequences of ejecta blanketing, such as topographic smoothing, are easily mistaken with space weathering. Thus, ejecta blanketing is not usually considered as the main scenario explaining the deficit in small craters.

[9] Ejecta blanketing has been simulated by Richardson et al. [2005] on the basis of seismic shaking modeling using an approach adapted from lunar crater studies. The expression used by Richardson et al. [2005] for simple ejecta blanketing modeling assumes that crater formation occurs in the gravity regime, which is appropriate for the Moon, but not really for low-gravity asteroids. In the method of Richardson et al. [2005], erasure occurs in limited areas of 5 crater radii from the impact location. In the present study, we focus on a reassessment of the effects of ejecta coverage by improving this simulation using an ellipsoidal model of the shape of Eros, with principal diameters of 34 km 16 km 12 km and a rotation period of about 5.27 h, following Miller et al. [2002]. We therefore take into account the aspherical gravity in the modeling of individual ejecta trajectories. Indeed, assuming that ejecta fall in the area delimited by 5 crater radii from the impact site is too simple for low-gravity bodies as ejecta can orbit around the asteroid before landing.

[10] A previous study about ejecta distribution has been performed by Korycansky and Asphaug [2004] on the basis of an accurate model of Eros composed of 1280 surface element faces. Their set of Monte Carlo simulations of the location of ejecta is based on two steps, the first distributing primary impacts randomly and the second integrating the orbits of test particle ejecta launched from primary impact locations. The distribution of ejecta has suggested that regolith tends to fill low-topography areas, denuding topography highs. Although the modeling performed in the present study is also based on primary impacts and secondary impacts of the ejecta blocks, it does not aim to produce a map of regolith thickness directly comparable to crater density on Eros. It rather computes a regolith blanket on an ellipsoidal model allowing the simulation of a global size-frequency distribution of the crater population, which we compare to that of Chapman et al. [2002] and Robinson et al. [2002]. To reach this goal, we focus on estimating a regolith production rate from different target characteristics (strong bedrock or porous regolith) as a function of time rather than trying to reproduce the regolith blanket for an accurate model of the shape of Eros. Then, although Korycansky and Asphaug [2004] aimed to study the ejecta

distribution on Eros, our goal is to simulate the ejecta coverage process that buries craters during the bombardment of Eros.

[11] We base our models on different exposure times to a main belt asteroid population. For each crater excavated, the trajectories of the ejecta are computed as well as their volume and landing location, allowing us to estimate the coverage effects.

[12] Our results somehow reduce the importance of seismic shaking, while not ruling it out, as a deficit in small craters remains. This shows that both effects must be modeled accurately before attempting to extract information about the interior of small bodies from modeling of the seismic shaking with potential site effects.

## 2. Modeling of Impact Cratering

[13] The crater population of Eros is quite similar to that of main belt asteroid Ida (which is nearly in saturation equilibrium), especially for the large crater population. Given this similarity, Chapman et al. [2002] suggested that asteroid Eros was in the same environment as Ida (the Main Asteroid Belt) when it acquired more than 99% of its cratering record. Its recent Mars-crossing orbit implies a negligible impact production. Therefore, we assume a main belt impacting population for Eros, as confirmed by the dynamical studies of Michel et al. [1998].

[14] The number of impacts expected in 1 year during a given bombardment period is estimated from equation 18 in the work of O'Brien et al. [2006]:

$$f = D_p^{-1/4} P_i \bar{r}_i^2 N_p(D_p) ; \quad (1)$$

where  $\bar{r}_i$  is the mean radius of the target asteroid (8 km for Eros),  $P$  corresponds to the intrinsic collision probability that applies to the specific size of asteroid Eros ( $2.86 \times 10^{-18} \text{ km}^2 \text{ a}^{-1}$ ), and  $N_p(D_p)$  is the impacting population function ( $N_p$  is the number of impactors within a given range of diameters centered on  $D_p$ ). This population has been modeled by O'Brien and Greenberg [2005] from the constraints given by observations of the surface of asteroids, the distributions of asteroid families, the preserved basaltic crust of asteroid Vesta, the cosmic ray exposure ages of meteorites and the cratering records observed on asteroids. The Yarkovsky effect is also included, leading to a slight decrease in the number of small asteroids of the main belt.

[15] The mean time between impacts can be inferred from equation (1) as a function of the impactor diameter (Figure 1). For example, a projectile of 1 m in diameter could impact Eros once in 100 years, while a large projectile of 84 m in diameter could impact Eros once in 200 Ma. For the 20 largest craters of Eros (Table 1) and with a standard estimation of the impactor diameter, an exposure time of a few billion years is required in order to have a significant probability of occurrence for the four largest craters. These large craters are however rare and cannot be modeled statistically. They could have occurred before the breakup of Eros, which is expected to have reset the cratering history of the surface of Eros [Chapman et al., 2002]. Moreover, the seismic waves generated by these very large craters produced ground accelerations possibly capable of levitating and possibly ejecting some fraction of the surface

Figure 1. Mean time between impacts on asteroid Eros as a function of impactor and crater diameter computed from O'Brien et al. [2006, equation 18] on the basis of the main belt asteroid population data of O'Brien and Greenberg [2005]. The 20 largest craters are represented by circles.

regolith [Ball et al., 2004], as the acceleration largely exceeded the local gravity. We will therefore focus our study on the more superficial regolith layer, associated to the youngest impacts (after the reset of the surface), and will not address the thickness of the older regolith layers, associated to these older impacts (before the reset of the surface). The effect of such a possible deep regolith layer on our results will however be discussed.

[16] In order to compare our simulations to those of Richardson et al. [2005], we simulated different main belt exposure times:  $T_{\text{exp}} = 200 \text{ Ma}$ ,  $T_{\text{exp}} = 400 \text{ Ma}$  and  $T_{\text{exp}} = 600 \text{ Ma}$  using projectiles with a maximum diameter of 84 m, 107 m and 137 m respectively, while the minimum diameter is 1 m in all simulations. These three impactor population lists (for the three different exposure times) are simulated on the basis of a random generator that selects a projectile diameter within a given range of diameters centered on  $D_p$ . Then, the random generator leads to different projectile diameters for each simulation, from the first to the last projectile. The location of the impact point of the projectile on the surface is also selected randomly.

[17] Such impactors have been used to assess the generation of craters and associated regolith on the surface of Eros. Following Richardson et al. [2005], a "cubed root" scaling-law has been adopted such that crater diameters  $D_c$  are proportional to the projectile diameter  $D_p$ :

$$D_c \propto D_p^{1/3} \quad (2)$$

For Eros, this relationship is an approximation for the diameter range of impactors considered in this study [Richardson et al., 2005]. The relationship between ejecta volumes and ejecta velocities is computed on the basis of a scaling law in the strength regime because of the small size of the simulated craters (the largest craters have a diameter of

Table 1. List of the Diameter of the 20 Largest Craters<sup>a</sup>

Crater Diameter (m)	Projectile Diameter (m)	Regolith Thickness (m)
10578	352.6	38
8150.9	271.7	17
5910.1	197	7
3599.1	120	1.5
3082	102.7	1
2465.6	82.2	0.5
1736	57.9	0.2
1624.6	54.2	0.1
1217.1	40.57	0.06
1114.6	37.2	0.05
1090.3	36.3	0.04
1038	34.6	0.038
1000.6	33.4	0.034
962.1	32.07	0.03
894.7	29.8	0.023
831.7	27.7	0.02
716.9	23.9	0.012
693.3	23.1	0.011
669.5	22.3	0.01
644.6	21.5	0.009

<sup>a</sup>Equivalent diameter of projectile calculated from equation (2) and the regolith thickness that the craters can produce on Eros, assuming impacts in a regolith target.

4 km). For each excavation velocity (lower than the Eros escape velocity of  $12 \text{ m s}^{-1}$ ) the volume of ejecta is estimated with the scaling relation from Housen et al. [1983]:

$$\frac{V_E}{R_c^3} \propto \frac{r}{v} \frac{r}{Y} v_e \quad (3)$$

The crater radius is  $R_c$ , the volume of ejecta excavated with a velocity lower than  $v$  is  $V_E$ ,  $r$  is the target density and  $Y$  the target strength.

[18] The density of impactors is chosen equal to  $3000 \text{ kg m}^{-3}$  (considering the typical density of a rocky body) and impact velocity is constant with a value of  $5300 \text{ m s}^{-1}$ , which is the mean impact velocity in the Main Asteroid Belt [Bottke et al., 1994]. The angle of impact is constant and equal to the most probable angle on a spherical object, i.e., 45 degrees (to be precise, this value is different on an ellipsoidal model but one can consider that this is a second-order effect). Our simulations account for the evolution of the regolith thickness with time ( $H_{cum}$ ), assuming that the falling ejecta blocks produce the regolith blanket. Then, two different physical parameters for the asteroid surface are assumed, depending on the current cumulated regolith thickness  $H_{cum}$ . If the impact occurs in the regolith layer (i.e., when the crater excavation depth is smaller than the current regolith thickness), we set the target characteristics to a dry soil [Holsapple, 1993], with a density of  $1700 \text{ kg m}^{-3}$  and strength of  $1 \cdot 10^5 \text{ Pa}$ . If the crater excavation depth is twice greater than the current regolith thickness  $H_{cum}$ , we assume an impact in a bedrock target with a soft rock characteristic: a density of  $2700 \text{ kg m}^{-3}$  and strength of  $1 \cdot 10^6 \text{ Pa}$ . This is an extreme case, in particular if an older regolith layer is present, for which values of the density and strength might be intermediate. Note however that an increase of the shear wave velocity from 100 m/s to 300 m/s has been reported on the Moon between these two regolith layers [e.g., Lognonné and Mosser, 1993] which

might be associated to a strength increase. The fresh regolith production, even for a large crater of 1 km in diameter, is only 2.1 times larger for a regolith impacted surface than for bedrock (Figure 2). Our approach will therefore minimize the production of fresh regolith compared to a more realistic model.

[19] These two cases will allow us to model the intermediate case, when the crater bottom starts to reach the bedrock, and while its depth is smaller than twice the regolith thickness we assume a crater formation in a dry soil target (regolith) and we set its depth to  $H_{cum}$  to produce a flat-floored crater [Quaide and Oberbeck, 1968].

[20] For a crater produced by a projectile of diameter greater than 10 m, the total volume is divided into an arbitrary value of 2000 fragments. These blocks are launched randomly along all directions (isotropic excavation) and the distribution of their launch velocity (which depends on the ejecta launch position) decreases from the center to the rim of the crater. Otherwise, for projectile diameters smaller than 10 m, we assume only one ejecta block excavated per crater, launched with a random azimuth and an average launch velocity. The average launch velocity is obtained from the arithmetic mean of the 2000 launch velocities calculated in the same way as for larger projectiles. These craters are so numerous that a good enough statistics is ensured for the fragments associated with the small projectiles. For exposure times of 200 Ma, 400 Ma and 600 Ma, 52%, 55% and 58% of the volume of reimpacted ejecta is provided by impactors with a diameter larger than 10 m. These large impactors account for 0.1% of the total impactor population and each projectile leads to 2000 ejecta blocks. As a result, 2/3 of the ejecta blocks are provided by impactors with a diameter larger than 10 m. The two kinds of impactors (with a diameter smaller or equal to 10 m or with a diameter larger than 10 m) then

Figure 2. Ejecta thickness produced in a surface of  $1125 \text{ km}^2$  (corresponding to the whole surface of Eros) by different crater sizes, for either a regolith or a bedrock target. The regolith target corresponds to dry soil characteristics with a density of  $1700 \text{ kg m}^{-3}$  and strength of  $1 \cdot 10^5 \text{ Pa}$ . The bedrock target has soft rock characteristics: a density of  $2700 \text{ kg m}^{-3}$  and strength of  $1 \cdot 10^6 \text{ Pa}$ .



produce approximately the same number of ejecta blocks, leading to a good statistical distribution.

[21] Ejecta trajectories are simulated within the gravity potential of Eros approximated by a massive rod in rotation. Indeed, the gravity potential of a 25 km massive rod matches closely (within a few percent) the gravity potential of an ellipsoid of constant density and of the total mass of Eros. This gravity potential can be expressed as:

$$U(p) = \frac{GM}{L} \coth^{-1} \frac{r_1 + r_2}{L} \quad (5)$$

where  $M$  is the mass of Eros ( $6.6904 \times 10^{15}$  kg, from Miller et al. [2002]),  $L$  is the length of the rod (25 km), and  $r_1$  and  $r_2$  are the distances from point  $p$  to each end of the rod. The impact locations are calculated from the intersection of the trajectories with a triaxial ellipsoid representing an approximation of the shape of Eros.

[22] For the three simulations with exposure times of 200 Ma, 400 Ma and 600 Ma, we simulate respectively  $3 \times 10^6$ ,  $6 \times 10^6$  and  $9 \times 10^6$  ejecta trajectories. For exposure times of 200 Ma, 400 Ma and 600 Ma, a total of 939,055 impactors, 1,878,120 impactors and 2,817,181 impactors, respectively, have been simulated. Only the ejecta trajectories intersecting the surface of the ellipsoid are taken into account for regolith formation. In all other cases ejecta either escape or are put into orbit.

[23] The banana shape of Eros could affect the pattern of intersecting ejecta by filling in the low-topography areas and denuding topography highs [Korycansky and Asphaug, 2004]. But in our study, which focuses on simulating the size-frequency distribution of the entire crater population of Eros, we will show later that taking regolith thickness variations into account would lead to similar results than assuming a homogeneous regolith thickness.

[24] The falling position of each ejecta block on the ellipsoid is computed and its volume is spread on the pixels around its landing site. The spreading law is an exponential function that decreases away from the landing location of the ejecta:

$$V_{cum} = A \exp(-d/l) \quad (6)$$

where  $H_{cum}$  is the cumulative regolith thickness,  $A$  is a factor such that the integration of this law gives the volume of the ejecta fragments,  $d$  is the distance to the reimpacting point, and  $l$  a length-scale value (taken equal to 700 m in practice). The values of ejecta volumes are then stored in a grid of latitude and longitude in which the cumulated ejecta thickness is computed (see Figure 4, section 3.1). In order to provide an estimate of the material volumes mobilized by impacts (Figure 2), a crater of 1 km formed in a bedrock target (soft rock characteristics) can produce an average regolith thickness of 1.1 cm, and an average regolith thickness of 2.4 cm when it is formed in a regolith target (dry soil characteristics). As shown in Figure 9 (section 3.4), regolith thickness therefore significantly affects the size-frequency distribution curve, and our approach (involving a strong bedrock beneath the regolith layer instead of a more compacted regolith beneath the regolith layer) underestimates the ejecta coverage effect of large craters by a factor of about 2. Any better model will have to take into

account all parameters associated with the impacts (including possible regolith ejection), as well as stratification in the regolith.

### 3. Results and Discussion

#### 3.1. Regolith Production

[25] According to Chapman et al. [2002] the cratering history of Eros has been reset during its breakup, and we assume that this breakup has ejected the uppermost fresh regolith from the surface. If we assume that most of this megaregolith is associated to the five largest craters, the thickness of this megaregolith can vary from 0 m (for a complete megaregolith ejection during breakup) to about 65 m (see Table 1 for the formation of regolith associated with these large impacts).

[26] With our hypothesis, the first impacts of the cratering history of Eros after breakup will follow the properties of impacts on bedrock, and their ejecta will cover either the bedrock or a primitive megaregolith layer. Later, ejecta accumulation depends on the properties of the impacted target and on regolith thickness at a given time. When the accumulating regolith blanket is thick enough, impacts occur in a regolith target with a dry soil characteristic. In all the simulations, the transition between impacts in bedrock and impacts in regolith occurs when the regolith thickness reaches about 3.7 m. Figure 3 shows that this is equivalent to about 50 Ma of impact history, possibly twice less if a megaregolith layer was present just after breakup. We will therefore consider this 50 Ma value as typical of our modeling error bar and note that the presence of primitive megaregolith will reduce this transition time, and therefore the associated error bar, by an extra regolith production before the transition.

[27] We have studied the global covering of the ejecta on the estimated surface ( $1125 \text{ km}^2$ ) of the asteroid for different exposure times (200 Ma, 400 Ma, and 600 Ma). This area of  $1125 \text{ km}^2$  differs slightly from the ellipsoid surface ( $1251 \text{ km}^2$ ) and is preferred for the estimation of the regolith thickness and crater population. Figure 3 shows that the simulations lead to a linear average regolith production, where the small sudden increases are related to major impact events. The slope is found to be equal to  $(H_{cum}/T_{exp}) = 7 \times 10^{-8} \text{ cm Ma}^{-1}$ . The production rate is slightly lower in the beginning, when the regolith thickness is smaller than 3.7 m: the cumulative regolith thickness is indeed created from a bedrock target, but this rate variation is negligible in the general trend. The general slope implies a regolith production rate of 1 m per 14 Ma, which corresponds to a cumulative regolith thickness created from craters excavated in a regolith target. This regolith accumulation with time leads to an average regolith thickness  $H_{cum} = 12 \text{ m}$  after an exposure time  $T_{exp} = 200 \text{ Ma}$ ,  $H_{cum} = 26 \text{ m}$  after an exposure time  $T_{exp} = 400 \text{ Ma}$  and  $H_{cum} = 40 \text{ m}$  for  $T_{exp} = 600 \text{ Ma}$  (Figure 3). The small differences in the shape of the production rate curves of Figure 3 are related to the different impactor sizes in the projectile populations impacting Eros. The average cumulative regolith thicknesses can also be computed from the regolith map (simulated from each ejecta fall) by summing the amount of material contained in each pixel. The regolith distribution on the ellipsoidal model is displayed in Figure 4 for an

Figure 3. Regolith thickness produced as a function of time for exposure times of  $T_{\text{exp}} = 200$  Ma,  $T_{\text{exp}} = 400$  Ma, and  $T_{\text{exp}} = 600$  Ma. The production rate is linear with a slope of  $H_{\text{cum}}/T_{\text{exp}} = 7 \times 10^{-8} \text{ m a}^{-1}$  and includes the evolution of the impacted target characteristics from a bedrock target to a regolith target.

exposure time  $T_{\text{exp}} = 400$  Ma. The computed average regolith thickness near the ends of the ellipsoid exhibits a small difference of 4% to 11% (depending on  $T_{\text{exp}}$ ) with respect to the rest of the model: there is a slight deficit in regolith on the ellipsoid ends, in agreement with Korycansky and Asphaug [2004]. Indeed, the study performed by Korycansky and Asphaug [2004] displays shaded contour maps of ejecta placement on Eros from their Monte Carlo calculations. Patterns of ejecta placement and of our regolith thickness map both highlight a slight deficit in regolith (linked to the ejecta falls locations) on the ends of the shape models used. Locations with a large thickness of regolith could correspond to low crater densities on the current surface, but claiming that there is a systematic correlation is not justified. Indeed, in the case of the Shoemaker crater, it has been shown (in the hypothesis of a formation after the breakup of Eros) that the crater degradation could be caused by seismic shaking associated with its creation [Thomas and Robinson, 2005], which reduces crater density in the vicinity of this large crater. The map obtained however shows significant lateral variations that must be taken into account in further studies together with the seismic shaking process [Richardson et al., 2005] to fully understand the geographical variations of crater density. Therefore let us focus on the average frequency-size distribution.

### 3.2. Calculation of Impact Crater Population by Ejecta Blanketing

[28] To test ejecta blanketing erasure of craters randomly located at the surface of the ellipsoid, we use a linear regolith production rate (Figure 3). For example, a crater located on a surface covered by a regolith thickness  $H_{\text{cum(surf)}}$  (known from the regolith map) will be subjected to a regolith coverage production rate  $H_{\text{cum(surf)}}/T_{\text{exp}}$ . To quantify ejecta coverage on a given crater, we check if the cumulative regolith thickness created by the following

impacts can bury that crater. Depending on its location on the surface of the ellipsoid, a crater will be subjected to different regolith production rates previously estimated from the regolith map. A crater is considered erased if covered by an ejecta thickness of one tenth of its diameter, which corresponds to the average depth of the crater [Richardson et al., 2005].

[29] When we simulate a given regolith distribution, we can distinguish further areas of the ellipsoid corresponding to extreme (high or low) regolith values (Figure 4). Then, each area is characterized by different production rates (that behave linearly with time). From Figure 4, we simulated the size-frequency distribution by selecting eight areas of different regolith production rates (craters that form in these areas undergo different burying rates related to different regolith production rates). We compare this size-frequency distribution with a size-frequency distribution based on a global regolith production rate (i.e., in which craters undergo the same average burying rate everywhere). As an example, we chose an exposure time  $T_{\text{exp}} = 400$  Ma. The results represented in Figure 5 display very similar curves, when testing a crater population accounting for the different production rates and a crater population accounting for an average production rate. This test suggests that in order to reproduce the size-frequency distribution of the craters of the entire Eros surface we do not need to take local variations of the regolith thickness into account for ejecta coverage. Therefore, we simplify our simulations by using the same production rate (based on the average regolith thickness) for all the craters on the ellipsoidal model independently of their location.

### 3.3. Comparison With the Observed Crater Population of Eros

[30] As a last step, the simulated crater population is compared to the observed crater population of Eros. Although it is not possible to correlate the local crater population on the basis of data for reasons cited above, we can compare the global simulated crater population to the observed crater population curve. Figure 6 shows the cumulative distribution plot based on the modeled and observed crater size-frequency distributions (Chapman et

Figure 4. Map of ejecta volume deposition, producing a regolith blanket. The exposure time is  $T_{\text{exp}} = 400$  Ma, and 5,993,602 ejecta trajectories have been computed. The total average regolith thickness obtained is 26 m. The two areas represented by black frames correspond to the surfaces with extreme regolith values used to compute the size-frequency distribution of Figure 9.

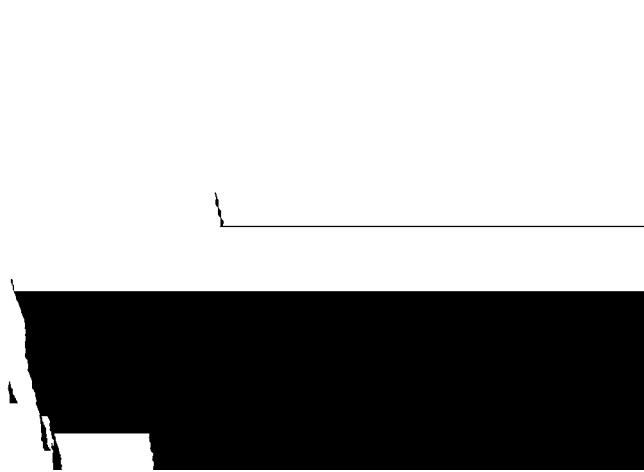


Figure 5. Size-frequency distribution for an exposure time  $T_{exp} = 400$  Ma. The dotted line is obtained from a heterogeneous regolith thickness (eight zones with a different regolith thickness have been assumed), and the solid line is obtained for an average regolith thickness of 26 m.

al. [2002] and Robinson et al. [2002] for the observed population) with the different exposure times considered above. These plots exhibit a good agreement between the simulated and the observed crater populations for main belt exposure times of 400 Ma and 600 Ma, in particular for crater diameters greater than 100 m. For smaller crater sizes, it appears that ejecta coverage does not involve enough regolith material to explain their observed deficit. Figure 7 represents the percentage of buried craters (compared to the initial crater population without erasure) as a function of



Figure 6. Cumulative size-frequency distribution plots of Eros craters per square kilometer as a function of crater diameter, displaying a best agreement between the observed and modeled populations after main belt exposure times of 400 Ma and 600 Ma. Note that Eros has a surface of  $1125 \text{ km}^2$  and that 13 craters have a diameter larger than 1 km.

Figure 7. Percentage of erased craters for different exposure times:  $T_{exp} = 200$  Ma,  $T_{exp} = 400$  Ma, and  $T_{exp} = 600$  Ma. This percentage has been estimated by comparison to the initial crater population simulated without erasure. The longest exposure time leads to a higher percentage of erased craters, affecting in particular the smallest ones.

their size, for the different exposure times considered, and shows that ejecta coverage significantly affects only the smallest craters. The smallest craters are easier to bury because of their shallow depth, thus 70%, 85% and 90% of the craters larger than 30 m of diameter are filled for exposure times of 200 Ma, 400 Ma and 600 Ma, respectively. Generally, for a given crater size, a higher percentage of erased craters is obtained by a longer exposure time because a thicker regolith blanket is formed. The percentage of filled craters decreases for larger crater sizes, up to a critical diameter corresponding to the largest crater erased. This critical diameter is 105 m for  $T_{exp} = 200$  Ma, 260 m for  $T_{exp} = 400$  Ma, and 420 m for  $T_{exp} = 600$  Ma. Figure 8 displays the cumulative distribution plot for the simulated crater population in the case of an exposure time of 400 Ma, which can be compared to that of Richardson et al. [2005]. The dashed line corresponds to the simulated crater population with erasure by ejecta blanketing, the solid line corresponds to the simulated crater population without erasure, and the dot-dashed line represents the simulated crater population of Richardson et al. [2005], including both a seismic shaking model and a simple ejecta blanketing model. The comparison between the solid and the dashed line suggests that for  $T_{exp} = 400$  Ma, the population of craters larger than 250 m can match the observed crater population independently of ejecta coverage erasure. Then, Figure 8 shows that ejecta coverage does not bury craters larger than 250 m for  $T_{exp} = 400$  Ma.

[31] Figure 8 also suggests that for craters larger than 30 m (for which our simulations do not fit the observed data well), ejecta coverage can bury a cumulative number of 900 craters out of 1000 per square kilometer, although the simulation of Richardson et al. [2005] (which is in agreement with the data), leads to a cumulative number of 980 filled craters per square kilometer. Even if it cannot explain all the small crater population, ejecta blanketing erasure has

Figure 8. Cumulative size-frequency distribution plots of Eros craters per square kilometer as a function of crater diameter for a main belt exposure time of 400 Ma. The comparison of the simulated crater population erased by ejecta coverage with the nonerased crater population shows that craters larger than typically 250 m in diameter are not filled by ejecta burial. Therefore, erasure by seismic shaking remains necessary to explain the observed crater population. The symbols used are listed in Table 1 of Chapman et al. [2002].

a nonnegligible effect and contributes to more than 50% of the erosion of small craters.

### 3.4. Effect of Regolith Thickness on Size-Frequency Distributions of Craters

[32] In order to understand the effect of ejecta coverage on size-frequency distribution of crater populations, we plot local crater size distribution characterized by the extreme values of regolith thickness (17.5 m and 53 m; see Figure 9. The location of these two areas is shown in Figure 4). Figure 9 allows us to compare the crater population with and without ejecta coverage erasure for these two areas that have a quite similar initial crater population (without ejecta coverage). First, one can see that even if the crater populations of these small areas do not include large craters as in the entire Eros crater population (large craters are rare in small areas), the slope of the curves is similar to the slope for the entire crater population. Second, when considering erasure, the surface covered by 53 m of regolith exhibits a deficit in all crater sizes (they are easily buried by the thick regolith blanket), although the surface covered by 17.5 m of regolith shows a crater population closest to the observed data set.

[33] Then, the local size-frequency distribution of Eros craters shows different trends depending on the local regolith thickness; but, as suggested in Section 3.2, taking local regolith thickness variations into account leads to the same crater population as when using an average regolith thickness. This test shows that the crater population curve of a given surface is very sensitive to regolith thickness and that a good fit can be achieved only for the complete surface.

[34] When local size-frequency distributions (that can be inferred by counting local craters) become available, it may be possible to compare them directly with our simulations.

## 4. Conclusions

[35] One of the new results of this work is that ejecta blanketing has an important contribution to crater erasure (for an exposure time of 400 Ma, it could bury up to 85% of crater sizes ranging between 30 m and 250 m), while the role of seismic shaking remains important.

[36] As shown by the observation of the numerous blocks present in the largest craters of Eros [Thomas et al., 2001] and by the smooth landscape images provided by the NEAR spacecraft, ejecta coverage can affect craters of any size without burying them. Indeed, we suggest that only the smallest craters with a diameter lower than typically 105 m to 350 m, for an exposure time ranging from 200 Ma to 600 Ma respectively, can be buried.

[37] One of our numerical simulations performed with an exposure time of 400 Ma is in good agreement with the data and therefore suggests a surface reset about 400 Ma ago.

[38] The deficit in large craters of the simulations and also the deficit in craters with a diameter between 0.5 km and 1 km (Figure 6) is however clearly linked to an older age of the bulk of Eros. Indeed, a significant probability for the largest impacts (Himeros, Shoemaker, Psyche, etc.) in the last 400 Ma requires a variable impactor flux, as suggested by Michel et al. [1998], but will nonetheless lead to a higher regolith thickness and therefore to a lower exposure time.

[39] The same is true for a long exposure without regolith surface reset: it will statistically support the presence of

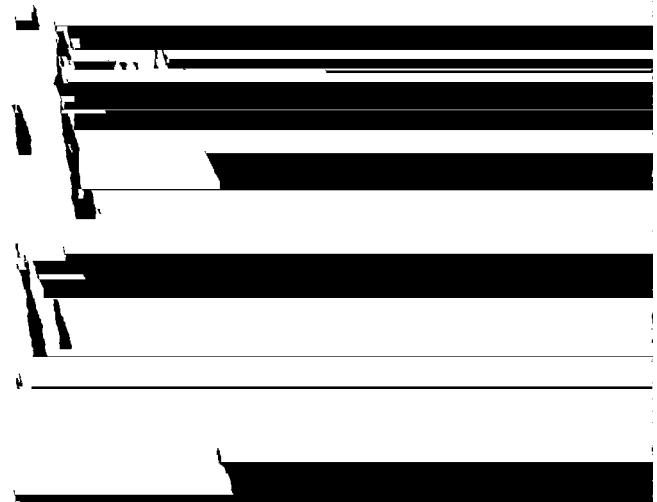


Figure 9. Size-frequency distribution of craters located in two small areas for an exposure time of 400 Ma. One area is covered by a thin regolith of 17.5 m, and the other is covered by a thicker regolith of 53 m (the location of these two areas is shown in Figure 4). The curves are computed for cases with and without ejecta coverage erasure. The solid line corresponds to the crater population on the entire asteroid surface without erasure.



large impacts, but on the other hand will imply a very thick regolith, much larger than 50 m, which again will require a lower exposure time. In all cases however, our results do not affect the main conclusion suggesting nonnegligible effects of the ejecta blanketing process.

[40] We therefore prefer to consider that the largest craters (Himeros, Shoemaker, Psyche, etc.) predate the breakup of Eros, and that this breakup or one of these large impacts has reset the surface of Eros.

[41] Our results then support the idea that this breakup or very large impacts occurred about 400 Ma ago and was/were associated with the ejection of most of the uppermost surface regolith, with the possible exception of the largest blocks of the megaregolith.

[42] This hypothesis of an older body is supported by Chapman et al. [2002], suggesting a 2 Ga age for Eros from the similarity between the crater populations of Eros and Ida (whose cratering age has been estimated at 2 Ga [Chapman, 1996]).

[43] We have also shown that the size-frequency distributions of the crater populations are very sensitive to regolith thickness, and the value of 26 m or 40 m of fresh regolith (not the possible megaregolith predating the breakup), obtained with exposure times of 400 Ma and 600 Ma, shifts the simulated crater population curve close to the observed crater population. These average cumulative regolith thicknesses are within the range of the regolith thickness proposed by Robinson et al. [2002], who compared the depth of the fresh craters to the depth of the degraded craters and inferred values ranging from a few meters to approximately 150 m. The maximum regolith thickness value (70 m) simulated with an exposure time of 400 Ma is however less than twice lower than the maximum regolith thickness suggested by Robinson et al. [2002] (150 m). This difference can also be linked to topographic effects on Eros that could explain high accumulations of regolith highlighted by data analysis and confirmed by Korycansky and Asphaug [2004]. The simulated regolith thicknesses of fresh regolith are also consistent with another estimation of Robinson et al. [2002] based on crater volumes, which suggested a regolith thickness ranging from 20 m to 40 m.

[44] If the five largest craters predate the breakup of Eros, we can add the occurrence of a megaregolith layer (up to a maximum of 65 m) beneath the fresh regolith formed with smaller craters to our estimates of 26 m or 40 m of fresh regolith.

[45] Ejecta coverage has an important contribution to crater erasure (in particular for the smallest craters), but it does not produce enough regolith to be the only phenomenon responsible for the observed deficit in small craters. As suggested by Richardson et al. [2005], erasure by seismic shaking is clearly responsible for part of the lack of small craters (evidence of downslope movement is visible on crater walls [Robinson et al., 2002]), but we have shown that it is probably not the only process (let us mention that the simulation of Richardson et al. [2005] also includes an ejecta blanketing model). In reality, crater erasure likely corresponds to a combination of different processes, including at least seismic shaking, ejecta blanketing, and probably, electronic dust levitation [Asphaug, 2004]. These effects will have to be modeled accurately in future work in order

to use the size-frequency curves as an indication of the regolith thickness of small bodies. Seismic shaking, for instance, could be modeled accurately, taking the complex shape of Eros into account, on the basis of the spectral-element method [e.g., Komatitsch et al., 2001; Martin et al., 2008].

[46] Acknowledgments. The authors thank Olivier Barnouin-Jha for kindly providing the scaling laws to compute ejecta characteristics and the data of crater diameters on Eros and David P. O'Brien and William F. Bottke Jr. for providing the main belt impactors data set. They are grateful to Keith A. Holsapple and Michael C. Nolan for fruitful discussion and to anonymous reviewers whose comments improved the manuscript. This research was supported by the French Programme National de Planétologie, by an R&T project of CNES, France, and by European FP6 Marie Curie International Reintegration grant MIRG-CT-2005-017461. This is IPGP contribution 2490.

## References

- Asphaug, E. (2004), Nothing simple about asteroids, *Science*, 306, 1489–1492, doi:10.1126/science.1106674.
- Ball, A. J., P. Lognonné, K. Seifert, M. Pätzold, and T. Spohn (2004), Lander and penetrator science for near-Earth object mitigation studies, in *Mitigation of Hazardous Comets and Asteroids*, edited by M. J. S. Belton et al., chap. 13, pp. 266–291, Cambridge Univ. Press, Cambridge, U. K.
- Bottke, W. F., M. C. Nolan, R. Greenberg, and R. A. Kolvoord (1994), Velocity distributions among colliding asteroids, *Icarus*, 107, 255–268, doi:10.1006/icar.1994.1021.
- Bottke, W. F., D. P. Rubincam, and J. A. Burns (2000), Dynamical evolution of main belt meteoroids: Numerical simulations incorporating planetary perturbations and Yarkovsky thermal forces, *Icarus*, 145, 301–331, doi:10.1006/icar.2000.6361.
- Chapman, C. R. (1996), S-type asteroids, ordinary chondrites, and space weathering: The evidence from Galileo's fly by of Gaspra and Ida, *Meteorit. Planet. Sci.*, 31, 699–725.
- Chapman, C. R., W. J. Merline, P. C. Thomas, J. Joseph, A. F. Cheng, and N. Izenberg (2002), Impact history of Eros: Craters and boulders, *Icarus*, 155, 104–118, doi:10.1006/icar.2001.6744.
- Durda, D. D. (2004), Ejecta generation and redistribution on 433-Eros: Modeling ejecta launch conditions, *Lunar Plan. Sci.*, XXXV, abstract 1096.
- Holsapple, K. A. (1993), The scaling of impact processes in planetary sciences, *Annu. Rev. Earth Planet. Sci.*, 21, 333–373, doi:10.1146/annurev.ea.21.050193.002001.
- Horvath, P., G. V. Latham, Y. Nakamura, and H. J. Dorman (1980), Lunar near surface shear wave velocities at the Apollo landing sites as inferred from spectral amplitude ratios, *J. Geophys. Res.*, 85, 6572–6578, doi:10.1029/JB085iB11p06572.
- Housen, K. R., R. M. Schmidt, and K. A. Holsapple (1983), Crater ejecta scaling laws: Fundamental forms based on dimensional analysis, *J. Geophys. Res.*, 88, 2485–2499, doi:10.1029/JB088iB03p02485.
- Komatitsch, D., R. Martin, J. Tromp, M. A. Taylor, and B. A. Wingate (2001), Wave propagation in 2-D elastic media using a spectral element method with triangles and quadrangles, *J. Comput. Acoust.*, 9, 703–718, doi:10.1142/S0218396X01000796.
- Korycansky, D. G., and E. Asphaug (2004), Simulations of impact ejecta and regolith accumulation on asteroid Eros, *Icarus*, 171, 110–119, doi:10.1016/j.icarus.2004.03.021.
- Lognonné, P. (2005), Planetary seismology, *Annu. Rev. Earth Planet. Sci.*, 33, 571–604.
- Lognonné, P., and C. Johnson (2007), Planetary seismology, in *Treatise on Geophysics*, vol. 10, edited by G. Schubert, chap. 4, pp. 69–122, Elsevier, New York.
- Lognonné, P., and B. Mosser (1993), Planetary seismology, *Surv. Geophys.*, 14, 239–302, doi:10.1007/BF00690946.
- Martin, R., D. Komatitsch, C. Blitz, and N. Le Goff (2008), Simulation of seismic wave propagation in an asteroid based upon an unstructured MPI spectral-element method: Blocking and non-blocking communication strategies, *Lect. Notes Comp. Sci.*, 5336, 350–363.
- Michel, P., P. Farinella, and C. Froeschlé (1998), Dynamics of Eros, *Astron. J.*, 116, 2023–2031, doi:10.1086/300562.
- Miller, J. K., A. S. Konopliv, P. G. Antreasian, J. J. Bordi, S. Chesley, C. E. Helfrich, W. M. Owen, T. C. Wang, B. G. Williams, and D. K. Yeomans (2002), Determination of shape, gravity, and rotational state of asteroid 433 Eros, *Icarus*, 155, 3–17, doi:10.1006/icar.2001.6753.
- Morris, E. C., R. M. Batson, H. E. Holt, J. J. Rennilson, E. M. Shoemaker, and E. A. Whitaker (1968), Television observations from Surveyor VI, in

- Surveyor VI Mission Report. Part II: Science Results, Tech. Rep. 32-1262, pp. 9–45, Jet Propul. Lab., Calif. Inst. of Technol., Pasadena, Calif.
- Nakamura, Y., J. Dorman, F. Duennebier, D. Lammlein, and G. Latham (1975), Shallow lunar structure determined from the passive seismic experiment, *Earth Moon Planets*, 13, 57–66, doi:10.1007/BF00567507.
- O'Brien, D. P., and R. Greenberg (2005), The collisional and dynamical evolution of the main-belt and NEA size distributions, *Icarus*, 178, 179–212, doi:10.1016/j.icarus.2005.04.001.
- O'Brien, D. P., and R. Greenberg (2007), The lack of small craters on Eros is not due to the Yarkovsky effect, *Bull. Am. Astron. Soc.*, 39, p.512.
- O'Brien, D. P., R. Greenberg, and J. E. Richardson (2006), Craters on asteroids: Reconciling diverse impact records with a common impacting population, *Icarus*, 183, 79–92, doi:10.1016/j.icarus.2006.02.008.
- Quaide, W. L., and V. R. Oberbeck (1968), Thickness determinations of the lunar surface layer from lunar impact craters, *J. Geophys. Res.*, 73, 5247–5270, doi:10.1029/JB073i016p05247.
- Richardson, J. E., H. J. Melosh, and R. Greenberg (2004), Impact-induced seismic activity on asteroid 433 Eros: A surface modification process, *Science*, 306, 1526–1529, doi:10.1126/science.1104731.
- Richardson, J. E., H. J. Melosh, R. J. Greenberg, and D. P. O'Brien (2005), The global effects of impact-induced seismic activity on fractured asteroid surface morphology, *Icarus*, 179, 325–349, doi:10.1016/j.icarus.2005.07.005.
- Robinson, M. S., P. C. Thomas, J. Veverka, S. L. Murchie, O. S. Barnouin-Jha, and D. B. J. Bussey (2001), The geology of Eros, *Lunar Planet. Sci.*, XXXII, abstract 2134.
- Robinson, M. S., P. C. Thomas, J. Veverka, S. L. Murchie, and B. B. Wilcox (2002), The geology of 433 Eros, *Meteorit. Planet. Sci.*, 37, 1651–1684.
- Thomas, P. C., and M. S. Robinson (2005), Seismic resurfacing by a single impact on the asteroid 433 Eros, *Nature*, 436, 366–368, doi:10.1038/nature03855.
- Thomas, P. C., J. Veverka, M. S. Robinson, and S. Murchie (2001), Shoemaker crater as the source of most ejecta blocks on the asteroid 433 Eros, *Nature*, 413, 394–396, doi:10.1038/35096513.
- Thomas, P. C., et al. (2007), Hyperion's sponge-like appearance, *Nature*, 448, 50–56, doi:10.1038/nature05779.
- Yeomans, D. (1995), Asteroid 433 Eros: The target body of the NEAR mission, *J. Astronaut. Sci.*, 43(4), 417–426.
- D. Baratoux, Laboratoire de Dynamique Terrestre et Planétaire, Observatoire Midi-Pyrénées et Université Toulouse III, UMR5562, CNRS, 14, avenue Édouard Belin, F-31400 Toulouse, France.
- C. Blitz and D. Komatitsch, Laboratoire de Modélisation et d'Imagerie en Géosciences, Université de Pau et des Pays de l'Adour, INRIA Magique-3D, UMR5212, CNRS, Avenue de l'Université, F-64013 Pau, France. (blitz@ippg.jussieu.fr)
- P. Lognonné, Équipe Géophysique Spatiale et Planétaire, Institut de Physique du Globe de Paris, Université de Paris Diderot, UMR7154, CNRS, F-94100 Saint Maur des Fossés, France.